Low-cost synthesis of large graphene oxide flakes by the total oxidation of large natural graphite flakes

Zhang Yuanyuan[1,5], Mai Jianbin[2], Chen Wei[1,5], Zhang Wenlong[1,5], Liu Jing[1], Liao Huaping[1], An Junwei[3], Wang Jionghui[4], Huang Dongmei[4], Lv Wei[1,5,*], Du Hongda[1,5,*], Kang Feiyu[1,5]

(1. *Guangdong Provincial Key Laboratory of Thermal Management Engineering & Materials*, *Institute of Materials Research*, *Tsinghua Shenzhen International Graduate School*, *Shenzhen* 518055, *China*;
2. *State Key Laboratory of Precision Electronic Manufacturing Technology and Equipment*, *Guangdong University of Technology*, *Guangzhou* 510006, *China*;
3. *Inner Mongolia Qingmeng Graphene Technology Co. Ltd*, *Ulanqab* 012000, *China*;
4. *China Minmetals (Heilongjiang) Graphite Industry Co. Ltd*, *Hegang* 154100, *China*;
5. *Shenzhen Geim Graphene Center*, *National-Local Joint Engineering Laboratory of Functional Carbon Materials*, *Shenzhen* 518055, *China*)

Abstract: Large graphene oxide (LGO) sheets have significant advantages over smaller ones in various applications. However, producing them by the Hummers-type oxidation of large natural graphite flakes is challenging. The inherent limiting factors are generally believed to be that large graphite flakes are both difficult to oxidize fully and prone to fragmentation during the process. By in-situ monitoring the graphite oxidation, we observed that, given sufficient time, large graphite flakes may be fully oxidized while still remaining largely intact. Graphite oxidation is governed by diffusion of the oxidizer between the layers, and is described by Fick's law, where a high oxidizer concentration gradient increases the diffusion rate. We therefore increased the oxidizer concentration by minimizing the amount of solvent (concentrated H_2SO_4), achieving full oxidation of gram-scale large graphite flakes in a semi-solid state with significantly reduced reagent consumption. In addition, the reaction temperature was adjusted to balance graphite oxidation and Mn(VII) self-decomposition. Using this approach, gram-scale 200-, 100-, and 50-mesh natural graphite were all fully oxidized with a significantly reduced consumption of both H_2SO_4 and $KMnO_4$. A reduction in size occurs during exfoliation, yielding LGO with average sizes of 27.3, 58.7, 116.2 μm, respectively. This study not only provides a scalable and cost-effective strategy for LGO production but also advances the understanding of Hummers-type methods.

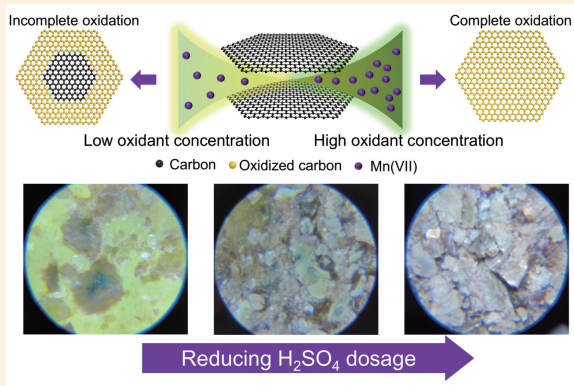

Key words: Large graphene oxide; In-situ monitoring; Oxidation; Oxidizer concentration

1 Introduction

The properties and applications of two-dimensional (2D) materials are strongly correlated to their lateral dimensions[1–2]. Graphene oxide (GO) is a crucial precursor for scalable graphene production and has great potential for numerous applications in nanocomposites[3–5], corrosion protection, biomedicine[6], energy storage and conversion devices[7], and thermal management[8–9]. The large-area GO (LGO) is particularly desirable for assembling dense coatings, and fibers or membranes with high mechanical strength, electrical and thermal conductivities[3,9–17]. However, producing LGO through Hummers-type oxidation of large-area natural graphite flakes has been considered to be challenging especially in large-scale industrial production, which results from 2 aspects: (1) The oxidation is typically considered to be controlled by dif-

Received: July 30, 2025
Revised: October 19, 2025
Accepted: October 20, 2025

fusion of oxidizer from the edges of the graphite to the cores[18–19]. When the size of the graphite flakes is large, the diffusion path for oxidizer is long, often resulting in flakes with oxidized edges but insufficiently oxidized cores[15,19–28]. (2) The oxidation process involves the insertion of oxygen-containing functional groups into the graphite lattice, which causes stress build-up and disrupts the planar structure and leads to the fragmentation of large flakes into smaller pieces[2,29].

A number of studies have focused on the producing of LGO with the Hummers-type oxidation method, as summarized in Fig. S1. In many works, the excessive oxidizer (*e.g.* 6-12 ∶ 1 for the mass ratio of $KMnO_4$ to graphite) was used to enhance the oxidation[23,25,30]. Furthermore, researchers employed large expandable graphite or expanded graphite as raw materials since highly accessible structures facilitate the mass diffusion of oxidizer into graphene layers[11,31–33]. However, most strategies are not welcome in large-scale production due to complex processes and heavy consumption of oxidizer, intercalating agents, solvent, thermal or electrical power.

In a typical Hummers-type method, graphite oxidation consists of three basic stages[18–19,34]. The first involves converting graphite into a stage-1 graphite intercalation compound (GIC). Under the action of oxidizer, GIC gradually transforms into pristine graphite oxide (PGO). Finally, PGO quickly transforms into graphite oxide upon contact with water, and then it is exfoliated into single-layered GO. The transformation from GIC to PGO is a bottleneck process. For the first time, this work conducts in-situ monitoring of the oxidation process in large-area graphite therefore enhancing understanding of its oxidation mechanism.

According to Fick's law, increasing the concentration gradient can enhance the diffusion driving force[35]. It can be tuned by either changing the Mn(VII) amount or the volume of the solution. This work reduced the solvent amount to increase the oxidizer concentration and facilitated its diffusion, achieving complete oxidation of large-area graphite. The temperature of the oxidation reaction of the Hummers process has been typically kept at 35 °C or higher to promote oxidation[23,36]. But high temperature also accelerates the self-decomposition of Mn(VII), reducing its utilization rate. Therefore, this work re-optimized the reaction temperature to balance these 2 reactions.

2 Experimental

2.1 Chemicals

200-, 100-, 50-mesh natural graphites were purchased from Aladdin. QD8 and QD9 natural graphites were purchased from Qingdao Shengtengda. H_2SO_4 and HCl were purchased from Dongjiang, while $KMnO_4$ was bought from Xilong. $Na_2C_2O_4$ and H_2O_2 (30%) were bought from Aladdin. All reagents were used as received without any pretreatment.

2.2 Oxidation of graphite

$KMnO_4$ was slowly added to H_2SO_4 and stirred at 8 °C for 2 h. Graphite was added to the dark green liquid and stirred for 1 h at 8 °C. Then the beaker was transferred to a water bath at the oxidation temperature with stirring until it became viscous. After a period of time, the liquid in the mixture was quickly extracted using a stainless steel lemon squeezer, and the Mn(VII) retention was determined by $Na_2C_2O_4$ titration. The remaining solid was dispersed into cold water, heated to 90 °C for 30 min, filtered, washed with dilute HCl and water, freeze-dried, and then tested by an element analyzer for its oxygen content.

2.3 Purification and exfoliation of graphite oxide to produce LGO

Graphite oxide was mildly dispersed in distilled water, and the mixture was allowed to stand for 2 h until the supernatant became clear, which was then poured off. The precipitate was washed for 3 more times through sedimentation to get purified expanded graphite oxide. To produce single-layered LGO, wet expanded graphite oxide was dispersed in distilled water (with a concentration of around 5 mg/mL). The obtained dispersion was mildly stirred at 200 r min^{-1} for 3 h and then sonicated for 10 min to obtain a single-layered LGO dispersion. Dry LGO was then collected through freeze-drying.

2.4 Measurement of GO yield

The weight of graphite and dry GO was recorded as M_G and M_{GO}, respectively. The yield of GO (Y_{GO}) was calculated by $Y_{GO} = (M_{GO}/M_G) \times 100\%$.

2.5 Measurement of Mn(VII) concentration

In the Mn(VII) self-decomposition experiments, $KMnO_4$ was dissolved in H_2SO_4 in an ice bath and the green solution was then divided into 3 equal parts. They were placed in 35, 25 and 15 °C water bath. Titration was conducted after a certain time using $Na_2C_2O_4$ to determine the residual content of oxidizer. In detail, 100 μL of green solution was mixed uniformly with 10 mL of 5 °C deionized water and this purple solution was titrated using a 75 °C 0.01 mol/L $Na_2C_2O_4$ aqueous solution to determine the content of Mn(VII). Three parallel titration experiments were carried out with the same conditions. The reaction occurring during the titration process is given as follows:

$$2MnO_4^- + 5C_2O_4^{2-} + 16H^+ \rightarrow 2Mn^{2+} + 10CO_2 \uparrow + 8H_2O$$

In the graphite oxidation experiments, 1 mL of the sample was withdrawn from the reaction mixture using a pipette, then quickly dispersed into 10 mL of 5 °C deionized water, and the solid substance was separated by filtration. This process was completed within 5 min and the titration was then performed.

2.6 Characterization

The oxidation process of graphite was monitored by a Kenko STV-120M portable microscope. X-ray diffraction (XRD) patterns were recorded on a Bruker D8 Advance X-ray diffractometer (Cu *K*α source, λ = 1.54 Å) with a scan rate of 20° min^{-1}. For observing LGO sheets, samples were observed using a Murzider M460 microscope. Atomic force microscopy (AFM) was performed on Bruker Dimension Icon. Raman spectra were obtained on the Horiba LabRam HR800 Raman system with an Ar laser source of 532 nm in a macroscopic configuration. Fourier Transform infrared spectra (FTIR) were acquired on a Thermo Scientific Nicolet iS20 FTIR spectrometer. X-ray photoelectron spectroscopy (XPS) spectra were collected using a PHI 5000 VersaProbe II spectrometer, and the raw data were calibrated using the standard C 1s peak (284.8 eV).

3 Results and discussion

3.1 In-situ monitoring oxidation of graphite flakes

There is currently no kinetic model that can perfectly simulate the graphite oxidation process. It is commonly agreed that the oxidation starts at the edges of the graphite flakes and proceeds toward the cores. The reaction rate may depend on factors including oxidizer concentration, graphite size, graphite shape, temperature and so on. To better understand the oxidation process of graphite flakes, we conducted in-situ monitoring of both Mn(VII) concentration and color change of graphite flakes using optical microscopy (OM). Three grams of $KMnO_4$ was dissolved into 1 mL of concentrated H_2SO_4, resulting in a dark green liquid. We designed a thin flat glass container, in which 0.1 g of 50-mesh natural graphite flakes was put in it (inset in Fig. 1a). Half a milliliter of the above liquid was dripped into the container and the oxidation processed immediately at 25 °C. The color changes of graphite near the liquid surface were observed through a coverslip using a microscope. The experiment was conducted multiple times, with the liquid being sampled at different times using pipettes, and the concentration of Mn(VII) in it was measured by titration using $Na_2C_2O_4$ solution. Mn(VII) comes from $KMnO_4$ and exists as Mn_2O_7 or MnO_3^+ in the oxidation process[37]. At the beginning of the oxidation, the concentration of Mn(VII) in the liquid was 1.46 mol/L. It gradually decreased over time, dropping to 0.051 mol/L after 60 h, after which it became too low to be measured by titration. Three typical graphite flakes with diameters around 300, 500 and 1000 μm were monitored, and their changes were tracked and photographed (Fig. 1b). Partially oxidized graphite flakes exhibit a typical fried egg structure, where the core blue and peripheral white represent the intercalated unoxidized part and the oxidized part, respectively. Three graphite flakes were completely oxidized after approximately 48, 60 and 72 h, respectively, demonstrating that under the same conditions, larger graphite flakes have slower oxidation kinetics. This aligns with previous understanding

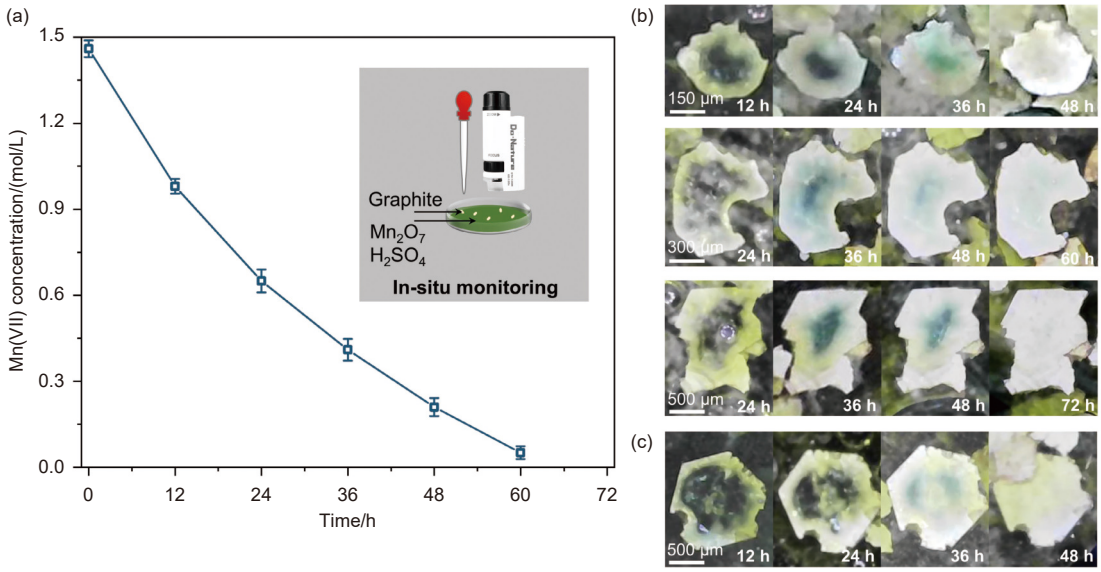

Fig. 1 (a) Monitoring of Mn(VII) concentration. In-situ monitoring oxidation process of (b) three graphite flakes with different sizes, and (c) graphite flake with cracks, where oxidation also processes from the cracks. Inset illustrates the in-situ monitoring method

that for large graphite flakes, a longer period is required for the cores to be oxidized. However, it is difficult for us to summarize the quantitative relationship between the time required for complete oxidation and the size of the graphite flakes, as well as the relationship between the concentration of oxidizer in the solvent and the rate of oxidation. Surprisingly, even after 60 h and with an extremely low concentration of oxidizer in the solvent, the oxidation reaction still proceeds. It can be explained that the change in graphite may lag behind Mn(VII) consumption due to the multi-step reaction mechanism in the oxidation process. Mn(VII) oxidizes graphite by generating reactive oxygen species (O_3, ·O· and HO·)[38]. At this magnification, on most graphite flakes' surface, we didn't observe new cracks formed during the entire oxidation process. Specifically, if the graphite flakes have inherent cracks, oxidation starts simultaneously from the edges and the cracks, continuing until the entire graphite is completely oxidized (Fig. 1c). Due to the presence of cracks, the lateral size decrease from graphite flakes to GO is usually significant. Strictly speaking, it is hard to determine how many cracks are generated during the oxidation process while how many are inherent in the graphite flakes. It is easy to speculate that in most Hummers-type methods, mechanical stirring may exacerbate the fragmentation of graphite flakes. Our monitoring indicates that in static oxidation, most large graphite flakes (with lateral size of up to 1 mm) can be completely oxidized while maintaining integrity, which diverges from the understanding presented in the majority of previous literature.

3.2 Complete oxidation of 100-mesh graphite

Based on the above understanding, we further explored suitable conditions for the bulk oxidation of graphite flakes. A typical experiment was conducted at 25 °C using 100-mesh graphite with an average lateral size of 194.0 μm (Fig. S2). Increasing the concentration of oxidizer may help facilitate the diffusion of oxidizer inside the graphite flakes, which may be realized by reducing the amount of solvent. However, a minimal amount of solvent is also essential to ensure mass transfer during the reaction. In order to study the effect of concentrated H_2SO_4 amount on graphite oxidation, the ratios of graphite mass (g), $KMnO_4$ mass (g), and H_2SO_4 volume (mL) were set to be 1 : 4 : 40, 1 : 4 : 30, 1 : 4 : 20 and 1 : 4 : 15, separately. Mn(VII) concentration in H_2SO_4 was monitored by titration. Meantime, partially oxidized graphite was sampled from the solution and observed with OM. These samples were then washed with cold water, filtered, and dried. The oxygen content of the dried samples was subsequently quantified using elemental

analysis (EA). As shown in Fig. 2a, reducing the amount of H_2SO_4 leads to a higher initial concentration of Mn(VII), but the concentration decreases more quickly, indicating that reducing the H_2SO_4 amount accelerates the consumption of Mn(VII). The oxygen content increased rapidly initially and then slowed down. Overall, the less H_2SO_4 is used, the faster the oxygen content in graphite increases, indicating that reducing the amount of H_2SO_4 accelerates graphite oxidation. However, in the later period of the reaction, the oxidation rate of the case with a raw material ratio of 1 ∶ 4 ∶ 15 significantly lagged behind other cases. After 48 h of reaction, the sample with a raw material ratio of 1 ∶ 4 ∶ 20 had the highest oxygen content (47.3%). The color of the graphite was observed at the 48 h (Fig. 2b-d). The sufficiently oxidized parts of the graphite flakes appear white (or contaminated by pinkish MnO_2), while the insufficiently oxidized parts appear blue[11,18–19]. In the cases of raw material ratios of both 1 ∶ 4 ∶ 40 and 1 ∶ 4 ∶ 30, insufficiently oxidized areas were observed in the cores of the graphite flakes. In the case of a raw material ratio of 1 ∶ 4 ∶ 20, the graphite flakes were entirely white, indicating that the graphite flakes had been completely oxidized. Due to the small amount of H_2SO_4, the mixture quickly turned into a semi-solid state after oxidation began (Fig. S3). While in the case of a raw material ratio of 1 ∶ 4 ∶ 15, large insufficiently oxidized areas were also observed (Fig. 2e), indicating that to ensure complete oxidation of the graphite, there is a minimum amount of H_2SO_4 required. The above experiments confirmed that by reducing the amount of H_2SO_4 and increasing the initial concentration of the oxidizer, the diffusion driving force of the oxidizer within graphite flakes is enhanced, promoting oxidation of the cores of the graphite flakes. However, if the amount of H_2SO_4 is reduced to a certain extent, as the oxidation reaction progresses, the graphite flakes swell and the H_2SO_4 will not be sufficient to fully infiltrate all the graphite flakes, ultimately resulting in incomplete oxidation of graphite.

The consumption of the Mn(VII) comes from both the graphite oxidation and the self-decomposition of Mn(VII). We determined the concentration changes of Mn(VII) through titration experiments and proved that the decomposition rate of Mn(VII) is highly influenced by temperature (Fig. 2f). Although it is commonly known that graphite oxidation rates increase with temperature[23,30,38], the simultaneous enhancement of Mn(VII) self-decomposition at elevated conditions complicates the process. The oxidation of large-area graphite is a prolonged process, during which the self-decomposition of Mn(VII) should not be ignored. Experimental optimization of temperature is crucial to balance these competing factors. A temperature of 35 °C was first adopted, referring to the original Hummers method[36]. The concentration of Mn(VII) decreased rapidly, while the oxygen content

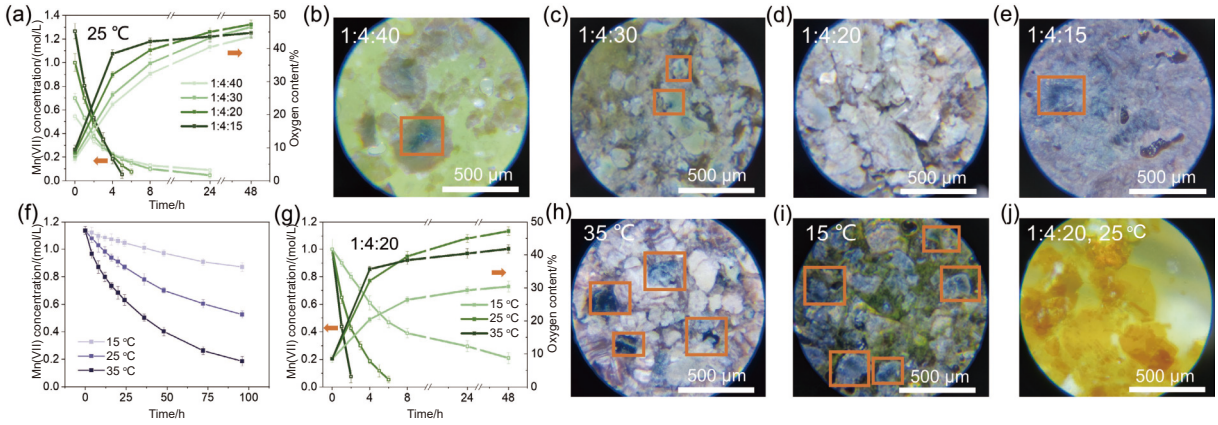

Fig. 2 (a) The change of Mn(VII) concentration and oxygen content of graphite over time with varying H_2SO_4 amount. (b-e) OM images of mixtures with different H_2SO_4 dosages at 48 h. (f) The self-decomposition rate of Mn(VII) in H_2SO_4 under different temperatures. (g) The change in Mn(VII) concentration and oxygen content of graphite over time under different temperatures. (h, i) OM images of mixtures (35 and 15 °C) at 48 h. (j) OM image of graphite oxide. The parts outlined by the orange-red boxes are the insufficiently oxidized domains

increased at a rate that was high initially but slowed down in the later stages (Fig. 2g). This indicates that in the later stage of the reaction, the oxidation drive was insufficient due to the extremely low concentration of Mn(VII). After 48 h, many insufficiently oxidized parts of the graphite were observed (Fig. 2h). To suppress the self-decomposition of Mn(VII) and improve its utilization on oxidation, lower temperatures (25 and 15 °C) were adopted. Lower temperature leads to slower consumption of Mn(VII) due to the deceleration of both oxidation and self-decomposition. As described earlier, graphite can be completely oxidized within 48 h at 25 °C. In case of 15 °C, the concentration of Mn(VII) remained at the highest level, but due to the weak graphite oxidation kinetics at 15 °C, the oxygen content has also remained at the lowest level. After 48 h, many insufficiently oxidized areas were observed (Fig. 2i). The oxidation reaction of graphite is a solid-liquid interface reaction driven by the diffusion of the oxidizer, and the temperature affects the reaction rate by influencing the diffusion coefficient of the oxidizer between the graphite layers. While the self-decomposition of Mn(VII) should be regarded as a homogeneous reaction in the solution, with the temperature directly affecting its reaction kinetics. These two reactions, with their sensitivity to temperature, compete and intertwine. Therefore, there is an optimal reaction temperature to balance them, which above experimental discussion suggests to be 25 °C. Overall, our experiments show that using a minimal amount of H_2SO_4 allows 100-mesh graphite to be completely oxidized at 25 °C within 48 h. To verify that all graphite flakes were completely oxidized, we sampled at 20 points throughout the mixture and observed no blue parts (Fig. S4, S5). After aqueous workup and heating, the obtained graphite oxide exhibits golden-yellow color and maintains its large, intact flakes with average size of 160.1 μm, slightly smaller than that of raw graphite flakes (Fig. 2j, Fig. S6).

3.3 Complete oxidation of graphite with different sizes

Due to the competition between the graphite oxidation and the self-decomposition of Mn(VII), more Mn(VII) may be wasted due to self-decomposition when oxidizing larger graphite of the same weight. Specifically, compared with 100-mesh graphite, oxidizing an equivalent mass of 200-mesh graphite requires less Mn(VII), while oxidizing an equivalent mass of 50-mesh graphite requires more Mn(VII). For 200-mesh and 50-mesh graphite (Fig. S7, average lateral size 86.6 μm and 0.65 mm), the mass ratios of graphite and $KMnO_4$ were set to be 1∶3.5 and 1∶4.5 to ensure that the Mn(VII) was in excess. Experiments were conducted at 25 °C to determine their minimum H_2SO_4 amount required for complete oxidation. For 200-mesh graphite, the ratios of graphite mass (g) and H_2SO_4 volume (mL) were set to be 1∶28, 1∶18 and 1∶13, separately. Its oxidation processes exhibited patterns similar to that of 100-mesh graphite. As shown in Fig. S8, reducing the amount of H_2SO_4 accelerates consumption of Mn(VII) and graphite oxidation. However, in the later period of the reaction, the oxidation rate of the case of 1∶13 lagged behind other cases (Fig. S8a). After 36 h of reaction, the case of 1∶18 had the highest oxygen content, which is 43.2%, while the graphite flakes were entirely white, indicating that the graphite flakes have been completely oxidized (Fig. 3a). In both cases of 1∶28 and 1∶13, insufficiently oxidized areas were observed in the cores of the graphite flakes (Fig. S8b, c). For 50-mesh graphite, the ratios of graphite mass (g) and H_2SO_4 volume (mL) were set to be 1∶45, 1∶35 and 1∶30, separately. Similarly, both Mn(VII) consumption and graphite oxidation sped up with reducing amount of H_2SO_4 but the oxidation rate of the case of 1∶30 lagged behind other cases (Fig. S9a). After 96 h of reaction, the case of 1∶35 had the highest oxygen content, which is 48.9%, while the graphite flakes were entirely white (Fig. 3b) while in both cases of 1∶45 and 1∶30, blue areas were observed (Fig. S9b, c). Overall, 1 g of 200- and 50-mesh graphite require minimum of 18 and 35 mL of H_2SO_4 to undergo complete oxidation. Our experiments indicate that for graphite of the same weight, the larger the size, the more H_2SO_4 is required for undergoing complete oxidation. It should be ascribed to that nat-

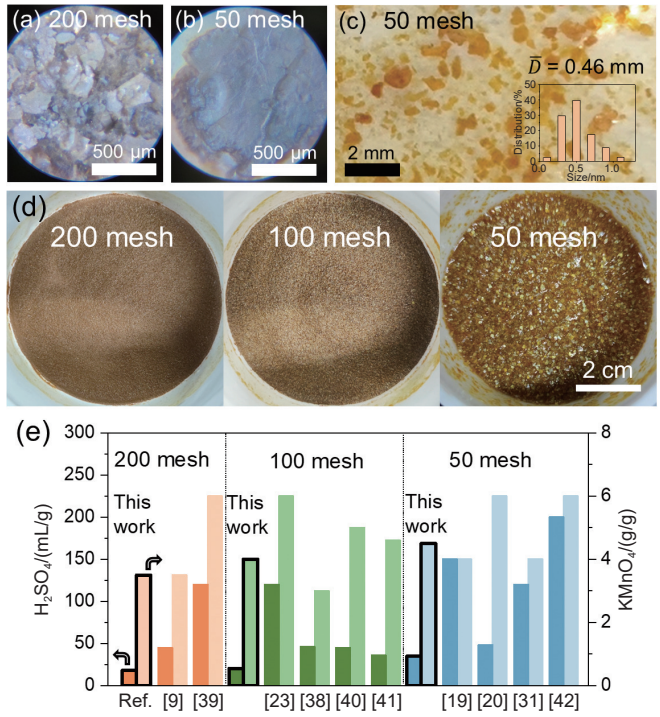

Fig. 3 (a) Completely oxidized 200-mesh graphite at 36 h. (b) Completely oxidized 50-mesh graphite at 96 h. (c) OM image and size distribution histograms of graphite oxide made from 50-mesh graphite. (d) Comparison of graphite oxide with different sizes. (e) Comparison of this work with reported methods for oxidizing large-area graphite in other literatures in terms of H_2SO_4 and $KMnO_4$ dosage

urally stacked larger oxidized graphite flakes of the same weight occupy a larger macroscopic volume than smaller one (Fig. S10).

After aqueous workup, the obtained GO flakes exhibit average size of 73.2 μm and 0.46 mm, respectively (Fig. S11, 3c), close to those of raw graphite. In general, by reducing amount of H_2SO_4, the oxidation rate of graphite can be enhanced and complete oxidation of most specification sizes of graphite can be achieved. Macrophotographs also show that most graphite oxide flakes remain intact (Fig. 3d), which provides a basis for the subsequent preparation of LGO. Another advantage is that amounts of H_2SO_4 and $KMnO_4$ consumed in this work are significantly less compared with most methods reported in literatures (Fig. 3e, Table 1)[9,19–20,23,31,38–42], which reduces costs and holds great significance for large-scale industrial production and environmental protection.

3.4 Exfoliation of graphite oxide to produce LGO

Graphite oxide was dispersed in water, allowed

Table 1 Comparison of this work with reported methods for oxidizing large-area graphite in other literatures in terms of H_2SO_4 and $KMnO_4$ dosage

Mesh number of graphite	Method	H_2SO_4 /(mL/g)	$KMnO_4$ /(g/g)
200 mesh	**This work**	**18**	**3.5**
	Modified hummers[9]	45	3.5
	Safer modified hummers[39]	120	6
100 mesh	**This work**	**20**	**4**
	Modified hummers[23]	120	6
	Water-enhanced oxidation[38]	46	3
	Pre-oxidation + Modified hummers[40]	45	5
	Taylor vortex flow[41]	35.8	4.6
50 mesh	**This work**	**35**	**4.5**
	Modified hummers[19]	150	4
	Modified hummers[20]	48	6
	Chemical expansion + Modified hummers[31]	120	4
	Intercalation + Thermal expansion + Modified hummers[42]	200	6

to fully swell (Fig. S12), and then exfoliated into LGO under gentle stirring[11,31,43]. LGOs obtained from 200-mesh, 100-mesh, 50-mesh graphite exhibited the average sizes of 27.3, 58.7 and 116.2 μm (Fig. 4a-c), respectively. The AFM images (Fig. 4d-f) validated that the thickness of LGOs is around 0.9 nm, indicating that they are single-layer[20,44]. The XRD patterns showed characteristic peaks centered at 2θ = 10.78°, 10.98° and 11.02° (Fig. 4g), corresponding to *d*-spacing of 8.21, 8.06 and 8.03 Å, respectively. As XRD was obtained from dry LGO, which was the product of restacking of LGO[19], the slightly decreasing *d*-spacing implies a higher degree of restacking due to increasing size[9,16]. The I_D/I_G values in Raman spectra of LGOs from 200-mesh, 100-mesh, 50-mesh graphite were 0.97, 0.95 and 0.92, respectively (Fig. 4h), which should be ascribed to that larger GO has fewer defects and higher carbon lattice integrity. In other literatures, the reported I_D/I_G ratio range of GO is commonly 0.92–1.23[11,33,45]. In comparison, the I_D/I_G ratio of GO in this work was at a relatively lower level, indicating that the LGO prepared in this study did not

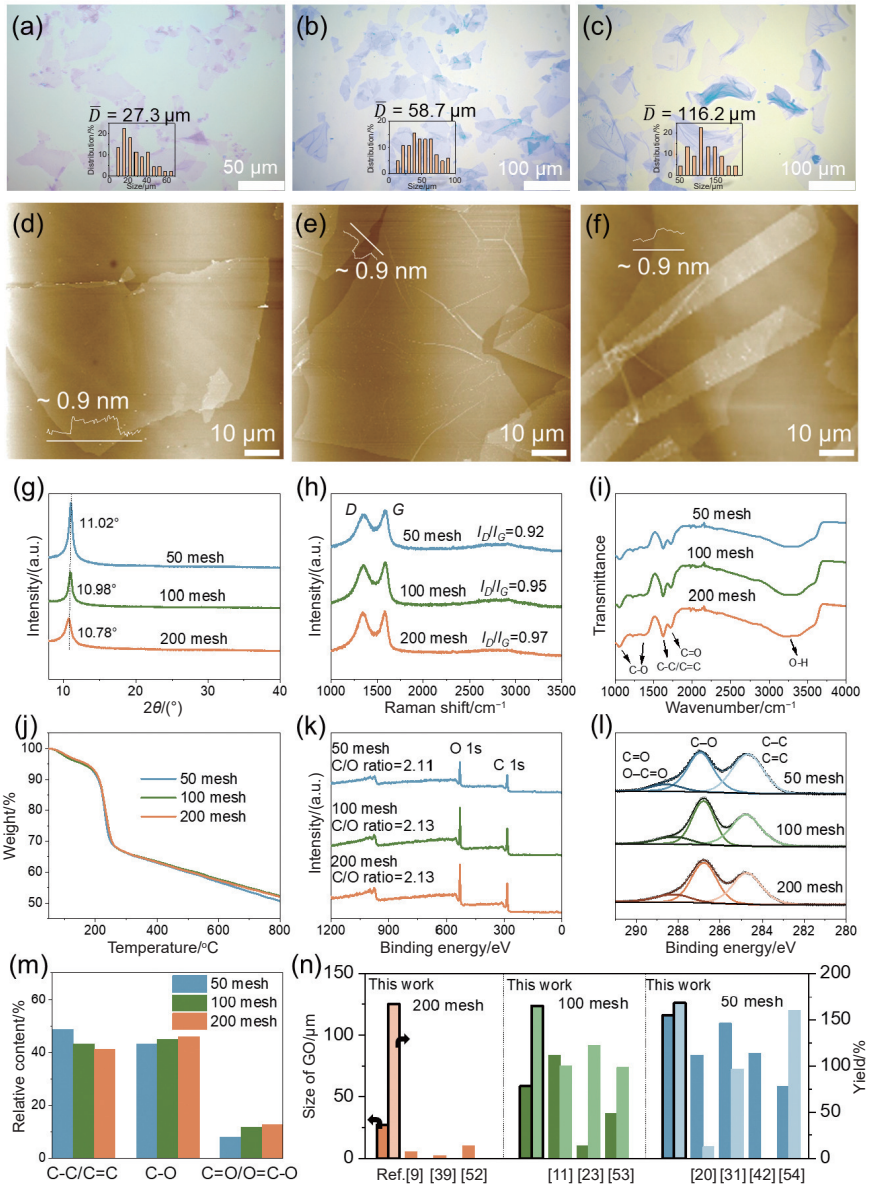

Fig. 4 Characterization of dry LGO: (a-c) OM images (on SiO_2/Si substrates), (d-f) AFM images (on mica substrates), (g) XRD patterns, (h) Raman spectra, (i) FTIR spectra, (j) TGA spectra, (k) XPS spectra, (l) XPS C1s spectra, and (m) relative content of groups. (n) Comparison of this work with reported methods for oxidizing large-area graphite in other literatures in terms of GO size and yield

exhibit over-oxidation. The FTIR identified the existence of similar functional groups including C—O (1045, 1250 and 1403 cm^{-1}), C=O (1716 cm^{-1}), C—C/C=C (1608 cm^{-1}) and—OH (3250 cm^{-1}) in three samples (Fig. 4i).[31,46] According to the thermogravimetric analysis (TGA) curves, LGOs synthesized from 200-, 100- and 50-mesh graphite showed similar thermal degradation curves between 50 and 800 °C (Fig. 4j), consistent with earlier EA data, where graphite oxide from 200-, 100- and 50-mesh samples showed oxygen contents of 43.2%, 47.3% and 48.9% respectively. XPS revealed slight differences in the carbon-to-oxygen (C/O) atomic ratio, measured at 2.13, 2.13 and 2.11, respectively (Fig. 4k). The XPS C 1s spectrum of LGO consisted of three types of carbon bonds: C—C/C=C (284.8 eV), C—O (286.9 eV) and C=O/O—C=O (288.6 eV) (Fig. 4l)[23,38,43,47–49]. The relative content of unoxidized carbon (C—C/C=C) increased with the lateral size of GO sheets, whereas the relative content of edge functional groups (C=O/O—C=O) in GO decreased with the same (Fig. 4m), indicating that larger GO sheets exhibit higher carbon lattice integrity and possess less edge functional groups[50–51]. Fig. 4n and Table 2 demonstrate that our work produced GO with larger sizes are comparable with most reported Hummers-type methods using graphite flakes of similar sizes, confirming its effectiveness in generating LGO. Additionally, our approach achieved a 100% conversion of graphite to GO and a yield exceeding 165%, surpassing values of most reported methods[9,11,20,23,31,39,42,52–54]. Specifically, our method produced the largest LGO among all reported methods that achieve 100% conversion of graphite to GO, which eliminated the need to separate the incompletely oxidized graphite from the product mixture by centrifugation or filtration[2,23,38].

In the aforementioned experiments, the natural graphite we used was sourced from the Aladdin brand, with a purity of 99.95%, which is among the most commonly employed natural graphite materials in scientific research. To validate the applicability of our method to natural graphite of varying purities and sources, we applied it to two additional types from Qingdao Tengshengda Carbon Co.: QD8 (80% purity; 63.2 μm average diameter) and QD9 (90% purity; 109.2 μm average diameter) (Fig. S13). The ratios of graphite mass (g), $KMnO_4$ mass (g), and H_2SO_4 volume (mL) were set at 1∶3.5∶16 and 1∶4∶18. After 30 and 44 h, respectively, both types of graphite were fully oxidized, yielding graphene oxide with average lateral sizes of 16.9 and 21.8 μm (Fig. S14). This demonstrates the broad applicability of our method for oxidizing diverse types of graphite.

Moreover, our method is applicable not only to the oxidation of large graphite flakes but also to that of small graphite flakes. Generally, oxidizing small graphite flakes can be easily achieved using the conventional modified Hummers' method. However, our proposed approach offers significant cost reduction

Table 2 Comparison of this work with reported methods for oxidizing large-area graphite in other literatures in terms of GO size and yield

Mesh number of graphite	Methods	Size of GO/μm	Yield/(%)
200 mesh	**This work**	**27.3**	**167**
	Modified hummers[9]	5.0	-
	Safer modified hummers[39]	2.0	-
	Modified brodie[52]	10.0	-
100 mesh	**This work**	**58.7**	**165**
	Chemical expansion + Modified hummers[11]	83.4	100
	Modified hummers[23]	10.0	122
	Chemical expansion + Modified hummers[53]	36.0	98
50 mesh	**This work**	**116.2**	**168**
	Modified hummers[20]	83.6	13
	Chemical expansion + Modified hummers[31]	109.7	96
	Intercalation + Thermal expansion + Modified hummers[42]	85.0	-
	Modified hummers[54]	58.3	160

while accomplishing the same process. To verify its applicability, we applied this method to 325-mesh graphite with an average lateral size of 28.5 μm (Fig. S15). The ratios of graphite mass (g), $KMnO_4$ mass (g), and H_2SO_4 volume (mL) were set to be 1∶3∶14. After 24 h, the graphite was completely oxidized. Upon exfoliation, GO with an average sheet size of 17.2 μm was obtained (Fig. S16), indicating that this method is also suitable for oxidizing small graphite and substantially reduces H_2SO_4 consumption compared with most reported methods[36,55–56].

It should be noted that increasing the amount of $KMnO_4$ can accelerate the oxidation process of graphite and reduce the time required for complete oxidation. Taking 100-mesh graphite as an example, when the amount of $KMnO_4$ was increased to 6 times that of graphite, with the ratios of graphite mass (g), $KMnO_4$ mass (g), and H_2SO_4 volume (mL) set to 1∶6∶20, the complete oxidation time at 25 °C was shortened to 30 h. However, due to the increased oxidizer concentration, the graphite flakes were more severely etched, resulting in both graphite oxide and GO with smaller average sizes of 107.8 and 39.8 μm, respectively (Fig. S17).

Although the oxidation process described in our method took a prolonged time, it was processed statically in a constant-temperature space with minimal energy input. Our method can be divided into 3 stages: stirring, static reaction, and aqueous workup. In large-scale production, these stages may be performed in 3 separate vessels: the stirring stage is conducted in a large reactor at low temperature over a period of several hours, the static reaction stage involves transferring the mixture into multiple portable small containers, which are then moved to a temperature-controlled room and allowed to stand for dozens of hours, and the aqueous workup stage is carried out by pouring the mixture into a large reactor containing cold water to complete the subsequent steps, a process that also requires several hours. In large-scale continuous production, 2 large reactors can be operated at full capacity by processing different batches of reactants in sequence, thereby maximizing equipment utilization. Those vessels used may be steel containers equipped with corrosion-resistant glass lining. Under such conditions, the overall production efficiency is primarily determined by the availability of adequate storage capacity rather than the duration of the reaction. Since such factories are typically located in remote areas where storage costs are relatively low, this proposed method remains cost-effective overall.

4 Conclusions

Large-area graphite flakes possess a long distance from the edge to the cores, making it difficult for oxidizer to diffuse, which leads to challenges in achieving complete oxidation. This study provides the first direct evidence that large graphite flakes (up to 1 mm) can be completely oxidized without fragmentation under static conditions, as shown by in-situ monitoring. Reduction of H_2SO_4 volume elevates oxidizer concentration, facilitating Mn(VII) diffusion through graphite interlayers and achieving complete oxidation. For a given size of graphite flakes, a minimum amount of H_2SO_4 is required to ensure complete infiltration and mass transfer during the entire oxidation process. Moreover, this work optimizes the temperature to balance the self-decomposition of Mn(VII) and the oxidation of graphite. Our experiments show that complete oxidation of 100-, 200-, 50-mesh graphite can all be achieved. Larger graphite flakes require a greater dosage of H_2SO_4 for complete oxidation because the naturally stacked volume in H_2SO_4 increases with size. Overall, LGO with average lateral sizes ranging from 27.3 to 116.2 μm was produced with conversion of 100% and yield over 165%. This study not only deepens understanding of graphite oxidation but also sheds new light on the development of LGO synthesis routes.

Acknowledgements

This work was supported by the National Natural Science Foundation of China (52372086), Open Bidding for Selecting the Best Candidates Program of Ulanqab City (2022JB005), Shenzhen Outstanding Talents Training Fund (RCJC20200714114436091), Guangdong Basic and Applied Basic Research Foundation (2023B1515120047), and Shenzhen Science and Technology Program Project (KJZD20230923114204008).

The authors would like to thank Testing Technology Center of Materials and Devices, Tsinghua Shenzhen International Graduate School for characterizations and measure-ments.

References

[1] Zavabeti A, Jannat A, Zhong L, et al. Two-dimensional materials in large-areas: Synthesis, properties and applications[J]. Nano-Micro Letters, 2020, 12(1): 66.

[2] Dong L, Yang J, Chhowalla M, et al. Synthesis and reduction of large sized graphene oxide sheets[J]. Chemical Society Reviews, 2017, 46(23): 7306-7316.

[3] Seyedin M Z, Razal J M, Innis P C, et al. Achieving outstanding mechanical performance in reinforced elastomeric composite fibers using large sheets of graphene oxide[J]. Advanced Functional Materials, 2015, 25(1): 94-104.

[4] Seyedin S, Razal J M, Innis P C, et al. Compositional effects of large graphene oxide sheets on the spinnability and properties of polyurethane composite fibers[J]. Advanced Materials Interfaces, 2016, 3(5): 1500672.

[5] Jin M, Jeong H-K, Yu W J, et al. Graphene oxide thin film field effect transistors without reduction[J]. Journal of Physics D: Applied Physics, 2009, 42(13): 135109.

[6] Lee J, Kim J, Kim S, et al. Biosensors based on graphene oxide and its biomedical application[J]. Advanced Drug Delivery Reviews, 2016, 105: 275-287.

[7] Hooch Antink W, Choi Y, Seong K-d, et al. Recent progress in porous graphene and reduced graphene oxide-based nanomaterials for electrochemical energy storage devices[J]. Advanced Materials Interfaces, 2018, 5(5): 1701212.

[8] Huang P, Li Y, Yang G, et al. Graphene film for thermal management: A review[J]. Nano Materials Science, 2021, 3(1): 1-16.

[9] Kumar P, Shahzad F, Yu S, et al. Large-area reduced graphene oxide thin film with excellent thermal conductivity and electromagnetic interference shielding effectiveness[J]. Carbon, 2015, 94: 494-500.

[10] Xu Z, Sun H, Zhao X, et al. Ultrastrong fibers assembled from giant graphene oxide sheets[J]. Advanced Materials, 2013, 25(2): 188-193.

[11] Dong L, Chen Z, Lin S, et al. Reactivity-controlled preparation of ultralarge graphene oxide by chemical expansion of graphite[J]. Chemistry of Materials, 2017, 29(2): 564-572.

[12] Wang N, Samani M K, Li H, et al. Tailoring the thermal and mechanical properties of graphene film by structural engineering[J]. Small, 2018, 14(29): 1801346.

[13] Malekpour H, Chang K H, Chen J C, et al. Thermal conductivity of graphene laminate[J]. Nano Letters, 2014, 14(9): 5155-5161.

[14] Wan Y J, Zhu P L, Yu S H, et al. Graphene paper for exceptional EMI shielding performance using large-sized graphene oxide sheets and doping strategy[J]. Carbon, 2017, 122: 74-81.

[15] Su C Y, Xu Y, Zhang W, et al. Electrical and spectroscopic characterizations of ultra-large reduced graphene oxide monolayers[J]. Chemistry of Materials, 2009, 21(23): 5674-5680.

[16] Yadav M K, Sangitra S N, Panwar N, et al. Aspect ratio dependent viscoelastic properties of graphene oxide liquid crystals[J]. Materials Chemistry and Physics, 2022, 287: 126305.

[17] Guo B, Liang G, Yu S, et al. 3D printing of reduced graphene oxide aerogels for energy storage devices: A paradigm from materials and technologies to applications[J]. Energy Storage Materials, 2021, 39: 146-165.

[18] Dimiev A M, Shukhina K and Khannanov A. Mechanism of the graphene oxide formation: The role of water, “reversibility” of the oxidation, and mobility of the C–O bonds[J]. Carbon, 2020, 166: 1-14.

[19] Dimiev A M and Tour J M. Mechanism of graphene oxide formation[J]. ACS Nano, 2014, 8(3): 3060-3068.

[20] Zhao J, Pei S, Ren W, et al. Efficient preparation of large-area graphene oxide sheets for transparent conductive films[J]. ACS Nano, 2010, 4(9): 5245-5252.

[21] Lin X, Shen X, Zheng Q, et al. Fabrication of highly-aligned, conductive, and strong graphene papers using ultralarge graphene oxide sheets[J]. ACS Nano, 2012, 6(12): 10708-10719.

[22] Jia J, Kan C-M, Lin X, et al. Effects of processing and material parameters on synthesis of monolayer ultralarge graphene oxide sheets[J]. Carbon, 2014, 77: 244-254.

[23] Marcano D C, Kosynkin D V, Berlin J M, et al. Improved synthesis of graphene oxide[J]. ACS Nano, 2010, 4(8): 4806-4814.

[24] Luo Z, Lu Y, Somers L A, et al. High yield preparation of macroscopic graphene oxide membranes[J]. Journal of the American Chemical Society, 2009, 131(3): 898-899.

[25] Wang S, Ang P K, Wang Z, et al. High mobility, printable, and solution-processed graphene electronics[J]. Nano Letters, 2010, 10(1): 92-98.

[26] Kim D W, Kim D, Min B H, et al. Sonication-free dispersion of large-area graphene oxide sheets using internal pressure from release of intercalated carbon dioxide[J]. Carbon, 2015, 88: 126-132.

[27] Zhou X and Liu Z. A scalable, solution-phase processing route to graphene oxide and graphene ultralarge sheets[J]. Chemical Communications, 2010, 46(15): 2611-2613.

[28] Lee W-J, Kim C-S, Yang S-Y, et al. Spontaneous exfoliation of large-sized graphene oxide with low defect concentration by simple wet chemistry[J]. Carbon, 2021, 182: 214-222.

[29] Pan S and Aksay I A. Factors controlling the size of graphene oxide sheets produced via the graphite oxide route[J]. ACS Nano, 2011, 5(5): 4073-4083.

[30] Li C, Shi Y, Chen X, et al. Controlled synthesis of graphite oxide: Formation process, oxidation kinetics, and optimized conditions[J]. Chemical Engineering Science, 2018, 176: 319-328.

[31] Zhang P, Zhou J, He P, et al. A one-pot strategy for highly efficient preparation of ultra-large graphene oxide[J]. Carbon, 2022, 191: 477-485.

[32] Zhang P, He P, Zhao Y, et al. Oxidating fresh porous graphene networks toward ultra-large graphene oxide with electrical conductivity[J]. Advanced Functional Materials, 2022, 32(42): 2202697.

[33] Wang X, Li X, Li A, et al. Synthesis of ultra-large diameter graphene oxide flakes from natural flake graphite[J]. Heliyon, 2024, 10(24): e40705.

[34] Nakajima T and Matsuo Y. Formation process and structure of graphite oxide[J]. Carbon, 1994, 32: 469-475.

[35] Tyrrell H. The origin and present status of Fick's diffusion law[J]. Journal of Chemical Education, 1964, 41(7): 397.

[36] Hummers W S, Jr. and Offeman R E. Preparation of graphitic oxide[J]. Journal of the American Chemical Society, 1958, 80(6): 1339-1339.

[37] Morimoto N, Suzuki H, Takeuchi Y, et al. Real-time, in situ monitoring of the oxidation of graphite: Lessons learned[J]. Chemistry of Materials, 2017, 29(5): 2150-2156.

[38] Chen J, Zhang Y, Zhang M, et al. Water-enhanced oxidation of graphite to graphene oxide with controlled species of oxygenated groups[J]. Chemical Science, 2016, 7(3): 1874-1881.

[39] Santamaría-Juárez G, Gómez-Barojas E, Quiroga-González E, et al. Safer modified Hummers' method for the synthesis of graphene oxide with high quality and high yield[J]. Materials Research Express, 2020, 6(12): 125631.

[40] Chen K, Tang X, Jia B, et al. Graphene oxide bulk material reinforced by heterophase platelets with multiscale interface crosslinking[J]. Nature Materials, 2022, 21(10): 1121-1129.

[41] Park W K, Yoon Y, Song Y H, et al. High-efficiency exfoliation of large-area mono-layer graphene oxide with controlled dimension[J]. Scientific Reports, 2017, 7(1): 16414.

[42] Nekahi A, Marashi P H and Haghshenas D. Transparent conductive thin film of ultra large reduced graphene oxide monolayers[J]. Applied Surface Science, 2014, 295: 59-65.

[43] Zhang J, Liu Q, Ruan Y, et al. Monolithic crystalline swelling of graphite oxide: A bridge to ultralarge graphene oxide with high scalability[J]. Chemistry of Materials, 2018, 30(6): 1888-1897.

[44] Stankovich S, Dikin D A, Piner R D, et al. Synthesis of graphene-based nanosheets via chemical reduction of exfoliated graphite oxide[J]. Carbon, 2007, 45: 1558-1565.

[45] He P, Zhou J, Tang H, et al. Electrochemically modified graphite for fast preparation of large-sized graphene oxide[J]. Journal of Colloid and Interface Science, 2019, 542: 387-391.

[46] Yuan H, Ye J, Ye C, et al. Highly efficient preparation of graphite oxide without water enhanced oxidation[J]. Chemistry of Materials, 2021, 33(5): 1731-1739.

[47] Chen J, Yao B, Li C, et al. An improved Hummers method for eco-friendly synthesis of graphene oxide[J]. Carbon, 2013, 64: 225-229.

[48] Yang D, Velamakanni A, Bozoklu G, et al. Chemical analysis of graphene oxide films after heat and chemical treatments by X-ray photoelectron and Micro-Raman spectroscopy[J]. Carbon, 2009, 47(1): 145-152.

[49] Pei S, Wei Q, Huang K, et al. Green synthesis of graphene oxide by seconds timescale water electrolytic oxidation[J]. Nature Communications, 2018, 9(1): 145.

[50] Zhang Q, Yang Y, Fan H, et al. Roles of water in the formation and preparation of graphene oxide[J]. RSC Advances, 2021, 11(26): 15808-15816.

[51] Sadasivuni K K, Kafy A, Zhai L, et al. Transparent and flexible cellulose nanocrystal/reduced graphene oxide film for proximity sensing[J]. Small, 2015, 11(8): 994-1002.

[52] Jeong S Y, Kim S H, Han J T, et al. High-performance transparent conductive films using rheologically derived reduced graphene oxide[J]. ACS Nano, 2011, 5(2): 870-878.

[53] Benzait Z, Chen P and Trabzon L. Enhanced synthesis method of graphene oxide[J]. Nanoscale Advances, 2021, 3(1): 223-230.

[54] Huang N M, Lim H N, Chia C H, et al. Simple room-temperature preparation of high-yield large-area graphene oxide[J]. International Journal of Nanomedicine, 2011, 6: 3443-3448.

[55] Chen J, Li Y, Huang L, et al. High-yield preparation of graphene oxide from small graphite flakes via an improved Hummers method with a simple purification process[J]. Carbon, 2015, 81: 826-834.

[56] Olumurewa K O, Olofinjana B, Fasakin O, et al. Characterization of high yield graphene oxide synthesized by simplified hummers method[J]. Graphene, 2017, 6(4): 85-98.